Available online at www.sciencedirect.com
SCIENCE DIRECT®
Journal of Sound and Vibration 288 (2005) 907–929
JOURNAL OF SOUND AND VIBRATION
www.elsevier.com/locate/jsvi

On the use of three-dimensional *h*- and *p*-version finite elements in solving vibration response problems

M. Dalenbring*, A. Zdunek

Swedish Defence Research Agency FOI, Aeronautics Division FFA, Computational Physics Department, SE-172 90 Stockholm, Sweden

Received 14 November 2003; received in revised form 26 November 2004; accepted 13 January 2005
Available online 29 April 2005

Abstract

The potential for reliably solving vibration response problems by using *h*- and *p*-versions of the finite element (FE) method is investigated. Each FE model is based on full three-dimensional (3-D) displacement-based continuum theory. Special attention is given to the ability to handle thin and/or nearly incompressible elastic and viscoelastic materials. Steady-state time-harmonic problems in the low- and mid-frequency ranges are treated. Convergence studies are performed on plate-like model problems with simply supported boundary conditions, using a series elasto-dynamic Navier solution extended to the viscoelasto-dynamic case by means of the elasto-viscoelastic correspondence principle. The importance of eliminating the discretisation error when using numerical solutions to estimate the frequency-dependent viscoelastic material parameters from experiments is stressed.

The superior efficiency of *p*-enrichments compared to *h*-refinements for resolving regular elastostatic solutions is observed in elasto/viscoelasto-dynamics as well. Requirements on *p*-enrichments to avoid shear- and volumetric locking are given. The frequently used polynomial interpolation functions employed are shown to produce a mass contribution to the dynamic stiffness, whose condition number deteriorates with increasing polynomial order. The practical implications and limitations of this observation are outlined. The recommended approach is corroborated using the measured frequency response on a laminate consisting of two aluminium plates and a constrained viscoelastic polymer damping treatment.
© 2005 Elsevier Ltd. All rights reserved.

*Corresponding author.
E-mail addresses: dgm@foi.se (M. Dalenbring), zka@foi.se (A. Zdunek).

0022-460X/$ - see front matter © 2005 Elsevier Ltd. All rights reserved.
doi:10.1016/j.jsv.2005.01.028

1. Introduction

Broadband high-frequency vibration analysis is important in many engineering applications. Traditionally, finite element (FE) models are based on low-order element interpolation and element *h*-refinements in order to get an accurate solution. However, this approach is limited to low-frequency analysis. The low-frequency range involves perhaps the first few 10 resonances and the vibration response is normally well predicted by using the standard *h*-version of the finite element method (FEM). Relying on the *h*-version FEM to solve vibration frequency responses leads to impractical mesh densities at sufficiently high frequencies in order to fulfill the Nyquist sampling theorem [1]. Today, high-frequency models are most often based on statistics and energy considerations. These approaches have other objectives, which are out of the scope of the present paper. A useful review of current analysis capabilities of mid- and high-frequency vibration predictions may be found in Ref. [2].

In order to manage mid-frequency FE analysis, alternative approaches need to be and can be adopted through an optimal use of element degrees of freedoms. The *p*- and *hp*-versions of the FEM offer such possibilities [3]. For a general presentation of the so-called higher-order FEMs, see Refs. [3,4]. These methods can advantageously be combined with a posteriori error estimation [5,6] upon which advanced automatic self-adaptive mesh refinement algorithms can be built [7]. The *hp*-version FE methodology can also alleviate locking problems encountered in traditional *h*-version FEM [8–10], and is thus a suitable candidate for solving also viscoelasto-dynamic problems, including nearly incompressible cases and cases involving thin layers.

The proper choice of the interpolation function set is of central importance in solving different problems with the *hp*-version FEM. It was soon realised that the use of a hierarchical interpolation function set, like the Legendre polynomials, is favourable in the sense that the functions with order p is a subset of order $p+1$ so that previously calculated orders of the mass and stiffness are untouched, which makes the process of approximation enrichment significantly faster. In addition, application-specific-type interpolation functions and improved integration by fast quadrature may also be utilised [11,12]. The usual polynomial set is less effective at higher frequencies as certain computational and numerical problems prevent the use of very high-order polynomial functions [13–18]. The trigonometric hierarchical interpolation function set offers better numerical stability at higher frequency. Beslin and Nicolas [14] use a 2-D trigonometric interpolation function set to calculate 800 eigenvalues with an error of less than 2%. The major disadvantage with this approach is that convergence at low-mode frequencies is not as good as for the polynomial interpolation set. A mixed polynomial and trigonometric interpolation function set is recommended for broadband frequency analysis [13,15,17]. The polynomial shape function set is used to describe element vertex degrees of freedoms and the trigonometric set is used to give additional freedom to the edge faces and the interior of the element. With proper use, the overall savings in computational cost is substantial and the next generation of commercial FEM codes will most likely be based on an *hp*-adaptive FEM methodology.

In the present paper, we restrict ourselves to a 3-D polynomial interpolation function set and low- to mid-frequency vibration response analysis, with damping included.

The modelling of damped linear systems considered here rests on the traditional three-dimensional (3-D) linear solid viscoelastic theory [19,20]. In practical applications, however, constant loss-factor models are often used for simulation of vibration responses despite the fact

that the material is highly frequency dependent and insufficiently represented by such a simple model. One explanation to the use of such oversimplified models could be lack of material data needed for damped materials like polymers and rubber. Another explanation may be that 1-D and 2-D approaches are still most common in vibro-acoustic applications. Moreover, only a few commercial FE code implementations are available for solving fully 3-D viscoelasto-dynamic problems. The 3-D approach, adopted in this paper, is strongly motivated by the fact that it is important to account for the 3-D state of stress and deformation in joint structures also at rather low frequencies [21]. These effects are especially important near boundaries and joints.

The process of experimental material damping estimation (Section 4) may also benefit from the use of *hp*-version FEM, suppressing the influence of discretisation error and providing means for optimal use of the degrees of freedoms. The process can be separated into two major parts: (a) estimation of discrete values of both real and imaginary parts of the material damping functions at each resonance frequency in the frequency interval of interest; (b) estimation of the viscoelastic model parameters. Modal models have been shown to be useful in material damping estimation [22–27]. To avoid truncation errors and modal coupling influence, an iterative estimation procedure using direct FE calculations with a general 3-D vibration response model proves favourable [28]. The use of direct FE is relatively computationally intensive. In estimation, however, these models are relatively small and only a few calculated frequencies are needed. In the second estimation step, the material damping function amplitudes are directly estimated by using the least-square damping approximation method, proposed in Ref. [24].

The major aim of this work is to put forward engineering guidelines for using a pure displacement solid continuum based approach for accurate and reliable numerical FEM simulations of 3-D time-harmonic linear viscoelasto-dynamic response problems in the low- and mid-frequency range. Special focus is put on guidelines for avoiding possible shear- and volumetric locking, by using proper enrichments of the polynomial interpolation order p. The p-version-type research code STRIPE used throughout here is referenced in Refs. [3,29] and further described in references therein.

One challenging practical target application is the modelling of the dynamic response of stiffened laminates, built up by thin layers of which some may be made of nearly incompressible linear viscoelastic materials (cf. Section 4).

The efficiency of p-enrichments compared to h-refinements is investigated for a given accuracy in the energy norm, in Section 3. The Nyquist sampling theorem requirements are investigated when using the p-version FEM approach. The polynomial interpolation functions often used will produce a mass-matrix contribution whose condition number deteriorates the dynamic stiffness with increasing polynomial order. This effect is investigated and practical implications and limitations of these observations are examined to find guidelines for required p-enrichments in order to avoid numerical problems.

2. Model problem formulation

2.1. The linear viscoelasto-dynamic vibration model problem

Consider the 3-D problem of finding the displacement field $\tilde{\mathbf{u}}(\mathbf{x}, s)$ at a point $\mathbf{x}$, given in Cartesian coordinates, in a Lipschitz domain, $\Omega \subset R^3$, subjected to tractions $\mathbf{g}$ on the boundary

$\partial\Omega$ of Ω, with no body forces present. Here, $s = \mathrm{i}2\pi f$ is the Laplace variable, $\mathrm{i}^2 = -1$ and f is the current frequency of vibration. The frequency domain Cauchy's first equation of motion is given in variational form as

Find $\tilde{\mathbf{u}} \in \mathbf{V} \in \mathrm{H}^1(\Omega) \times \mathrm{H}^1(\Omega) \times \mathrm{H}^1(\Omega)$ such that

$$B(\tilde{\mathbf{u}}, \tilde{\mathbf{v}}) = F(\tilde{\mathbf{v}}) \quad \forall \tilde{\mathbf{v}} = \mathbf{V}, \tag{1}$$

where $\mathbf{u}$, $\mathbf{v}$ are test functions in the Sobolev space H^1, B and F are sesquilinear and antilinear forms, respectively, defined as

$$B(\tilde{\mathbf{u}}, \tilde{\mathbf{v}}) = \int_\Omega \sigma(\tilde{\mathbf{u}}) : \tilde{\varepsilon}(\tilde{\mathbf{v}}^*)\, \mathrm{d}\Omega + s^2 \int_\Omega \rho \tilde{\mathbf{u}} \cdot \tilde{\mathbf{v}}^*\, \mathrm{d}\Omega, \tag{2}$$

$$F(\tilde{\mathbf{v}}) = \int_{\partial\Omega} \tilde{\mathbf{g}} \cdot \tilde{\mathbf{v}}^*\, \mathrm{d}\partial\Omega, \tag{3}$$

where * corresponds to a complex conjugate. The constitutive behaviour is modelled in the frequency domain by using a linear solid viscoelastic model, $\tilde{\sigma}(s) = \mathbf{C}(s) : \tilde{\varepsilon}(s)$.

The stresses $\tilde{\sigma}_{ij} = \tilde{\sigma}_{ji}$ and infinitesimal strains $\tilde{\varepsilon}_{kl} = \tilde{\varepsilon}_{lk}$ are symmetric second-order tensor fields with the strain–displacement relation, given as $\tilde{\varepsilon}(\tilde{\mathbf{u}}) = [(\nabla \otimes \tilde{\mathbf{u}})^{\mathrm{T}} + \nabla \otimes \tilde{\mathbf{u}}]/2$, where ∇ is the usual gradient operator and $\otimes$ is the dyadic product.

The solid viscoelastic model is defined by using N_a discrete relaxation processes. Each one is characterised by an internal tensorial strain field variable $\varepsilon_n^a(\mathbf{x}, t)$ and a corresponding modulus stiffness matrix $\mathbf{C}_n^a(\mathbf{x}, t)$. For this model, the stress response in $\sigma(\mathbf{x}, t)$ is defined by a 3-D constitutive relationship, where the initial (instantaneous, elastic) modulus stiffness matrix $\mathbf{C}^0$ is such that the strain energy $\varepsilon \cdot \mathbf{C}^0 \varepsilon > 0$ for an arbitrary ε. Each internal variable field ε_n^a is governed by the following evolution equation $\dot{\varepsilon}_n^a = 1/\tau_n(\varepsilon - \varepsilon_n^a)$, where each relaxation time $\tau_n > 0$ and the reference time, initial condition for vanishing internal strain ε_n^a, is set to $\lim_{t\to 0} \varepsilon_n^a(t) = 0$. The long-term elastic, fully relaxed, generalised Hooke's law modulus (a fully symmetric) fourth-order tensor $\mathbf{C}^\infty$ is defined to characterise all linear solids such that $\varepsilon \cdot \mathbf{C}^\infty \varepsilon > 0\ \forall \varepsilon$. The relation between the long-term elastic or fully relaxed modulus $\mathbf{C}^\infty$ and the instantaneous modulus is $\mathbf{C}^0 = \mathbf{C}^\infty + \sum_{n=1}^{N_a} \mathbf{C}_n^a$. Throughout this work a discrete relaxation spectrum is employed. The corresponding Laplace transformed (frequency domain) constitutive relation reads

$$\tilde{\sigma}(s) = \left[\mathbf{C}^\infty + \sum_{n=1}^{N_a} \frac{s \cdot \mathbf{C}_n^a}{s + \beta_n} \right] : \tilde{\varepsilon}(s) = [\mathbf{C}^\infty + \mathbf{C}_a(s)] : \tilde{\varepsilon}(s) = \mathbf{C}(s) : \tilde{\varepsilon}(s), \tag{4}$$

where β_n, $n = 1, 2, 3, \ldots, N_a$, are real positive relaxation frequencies with relaxation times $\tau_n = 1/\beta_n$. For connections with the so-called AHL theory, see Ref. [23].

An isotropic viscoelastic solid is defined by two independent moduli. Making use of the elasto-viscoelastic correspondence principle, we obtain $\mathbf{C}_a(s) = d_G(s) \cdot G\mathbf{C}_G + d_\lambda(s) \cdot \lambda \mathbf{C}_\lambda$, where non-zero components are $(\mathbf{C}_G)_{ii} = 1, i, k \leqslant 3$ and $(\mathbf{C}_\lambda)_{ik} = 2, 1 \leqslant i \leqslant 3$; $(\mathbf{C}_G)_{ii} = 1, \quad 4 \leqslant i \leqslant 6$. For N_a discrete relaxation processes, the isotropic material functions become $d_G(s) = \sum_{n=1}^{N_a} A_G^{(n)} \cdot s/(\beta_n + s)$ and $d_\lambda(s) = \sum_{n=1}^{N_a} A_\lambda^{(n)} \cdot s/(\beta_n + s)$, respectively, where $A_G^{(n)}$ and $A_\lambda^{(n)}$ are real process amplitudes with corresponding real positive relaxation frequencies β_n, $n = 1, 2, 3, \ldots, N_a$. Material functions for other material symmetries may easily be constructed by using the elasto-viscoelastic correspondence principle, cf. [19,20,25,26].

2.2. Frequency domain FE equations of motion and the associated eigenvalue problem

The solution to Eq. (1) may be approximated by a discrete set of equations using the FEM and a sequence of FE spaces, $\mathbf{V}^N \subset \mathbf{V}$. The discrete problem becomes: find $\tilde{\mathbf{u}}^N \in \mathbf{V}^N$ satisfying,

$$B(\tilde{\mathbf{u}}^N, \tilde{\mathbf{v}}) = F(\tilde{\mathbf{v}}) \quad \forall \tilde{\mathbf{v}} = \mathbf{V}^N, \tag{5}$$

with $B(\cdot,\cdot)$ and $F(\cdot,\cdot)$ given by Eqs. (2) and (3), respectively. The error of approximation is measured in the following energy-type norm, the Sobolev H^1 norm:

$$\|\tilde{\mathbf{e}}\|^2_{V^N} \equiv \int_\Omega \left|\tilde{\varepsilon} - \tilde{\varepsilon}^N\right|^2 + \left|\tilde{\mathbf{u}} - \tilde{\mathbf{u}}^N\right|^2 \mathrm{d}\Omega, \tag{6}$$

where $\tilde{\mathbf{e}} = \tilde{\mathbf{u}} - \tilde{\mathbf{u}}^N$ is the difference between the exact solution on strong form and a given FE approximation $\mathbf{u}^N$ to Eq. (1). See Ref. [6], for existence and uniqueness issues.

The steady-state-harmonic-forced frequency vibration response is obtained by direct solution of the FEM discrete equations of motion for a structure, with linear viscoelastic material properties, defined as

$$[\mathbf{K}_e + s^2\mathbf{M} + \mathbf{K}_a(s)]\tilde{\mathbf{U}}(s) = \tilde{\mathbf{F}}(s), \quad \mathbf{K}_a(s) = \int_\Omega \mathbf{B}^{\mathrm{T}}\mathbf{C}_a(s)\mathbf{B}\,\mathrm{d}\Omega, \tag{7,8}$$

where $\mathbf{M}$, $\mathbf{K}_e$ and $\mathbf{K}_a(s)$ are the usual mass, stiffness and complex frequency-dependent viscoelastic stiffness matrices corresponding to the global, generalised displacement degrees of freedom $\tilde{\mathbf{U}}$, while $\tilde{\mathbf{F}}$ is the corresponding global load vector, calculated by using an *hp*-version FE technique in a 3-D domain setting. $\mathbf{B}$ in Eq. (8) is the standard strain–displacement operator.

The corresponding eigenvalue value problem, given by elastic stiffness and mass matrices, is defined as

$$[\mathbf{K}_e + \lambda_m\mathbf{M}]\Psi_m = 0, \quad \Psi_m^{\mathrm{T}}\mathbf{M}\Psi_m = \delta_{mn}, \tag{9,10}$$

where λ_m is the eigenvalue (related to the eigenfrequency by $\omega_m^2 = \lambda_m$) and Ψ_m is the associated eigenvector, corresponding to a non-trivial solution to the equation system (Eq. (9)). The eigenvalue is a measure of the elastic modal strain energy and the error in the eigenvalue may be shown to be closely related to the square of a corresponding energy norm [3].

The set of modes is also the basis for the so-called modal analysis and forced vibration frequency response simulation by using modal superposition, cf. [22].

We use the *p*-version of the FEM to realise Eqs. (7) and (8), which enables us to effectively control the discretisation error by choosing an initial mesh (*h*-refinement) and then vary the polynomial (*p*-) enrichment. The continuum *p*-version hexahedral element in STRIPE used here may be described as follows. Usual Lagrangean nodal shape functions of second order are used to describe the geometry. Hierarchical polynomial basis functions of the Peano type [30,31] are used to describe the displacement. The polynomial order p may be between 1 and 15. Here, a spatially isotropic polynomial order is used in R^3, that is, $p = p_1 = p_2 = p_3$. Spatially anisotropic *p*-enrichments are possible and may be used to gain efficiency or to enforce a Mindlin-plate-type behaviour, see for example, Ref. [32].

3. A numerical study of simply supported flat plates

Vibration analyses of a number of realistic plates are used to show certain aspects of FE discretisation error control in terms of both elastic dynamic properties, that is, eigenvalues, and in terms of damped forced vibration frequency responses. An analytic 3-D series solution, cf. [33,34] and Appendix A are used to study the convergence between the exact solution and the FE approximation, with respect to variations in a priori h-refinements and p-enrichments. The percentage relative error is measured in the energy-type norm, Eq. (6). Simply supported boundary conditions are used throughout. The following elastic material data for Polymethylmethacrylate (PMMA) are used in the study: $E_{\mathrm{PMMA}} = 3440\,\mathrm{MPa}$, $\nu_{\mathrm{PMMA}} = 0.382$ and $\rho_{\mathrm{PMMA}} = 1181\,\mathrm{kg/m^3}$.

3.1. Elasto-dynamic analysis of a simply supported PMMA plate

In this section, eigenvalue analyses are used to investigate the convergence of the eigenvalues using different uniform polynomial approximations p and uniform h-refinements. For this purpose, a PMMA plate is used with simply supported boundary conditions and dimensions $1000 \times 1000 \times 10\,\mathrm{mm^3}$.

In Fig. 1, the convergence of FE approximated eigenfrequencies versus mode number is displayed for different orders of p using a 2×2 element FE model. The result obtained by the analytical 3-D series solution is also plotted (an almost straight line in Fig. 1) for comparison. The results in Fig. 1 clearly show that it is possible to calculate only a few eigenvalues with reasonable

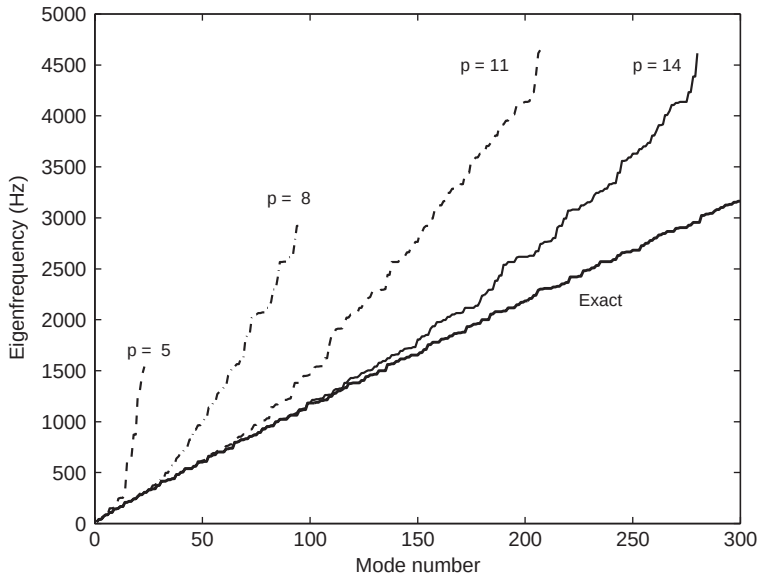

Fig. 1. Eigenfrequencies versus modal numbers for different FE approximations for different p-enrichments (5 dashed, 8 dashed–dotted, 11 thick dashed and 14 solid line) using a 2×2 elements model. Exact 3-D solution is also plotted for comparison (thick solid line).

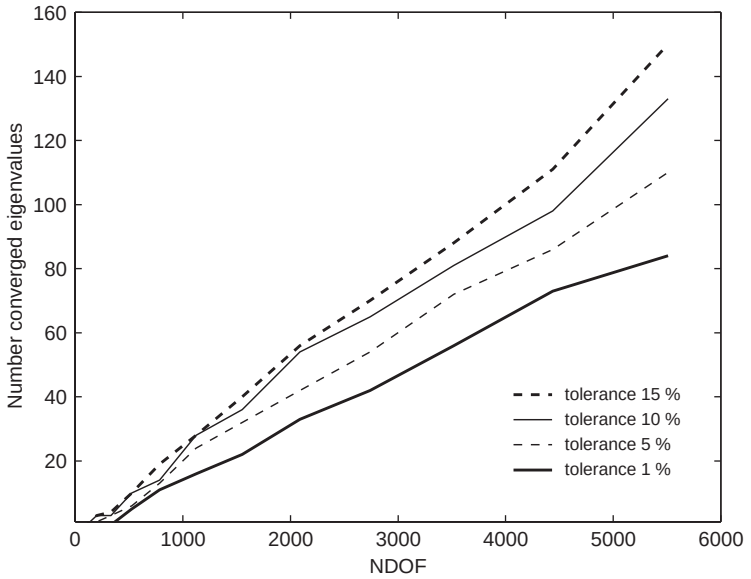

Fig. 2. Number of converged FE eigenvalues with respect to the exact solution versus number of used degrees of freedom (different orders of p and 2×2 elements) for different levels of tolerance in accuracy of the approximation (1% thick solid, 5% thin dashed, 10% thin solid and 15% thick dashed line).

accuracy by using the 2×2 element FE model, and p equals 5. However, we may calculate more than 100 eigenvalues with a fairly good accuracy by using p equals 14.

In order to display the effect of using uniform p-enrichments, the number of converged eigenvalues are plotted in Fig. 2 versus the number of degrees of freedoms used for different levels of tolerance. For comparison, the exact 3-D eigenfrequencies are also given in Table 1 for a selected number of wave numbers. Take mode number 90, for example. It has an eigenfrequency of 1047 Hz and modal wave numbers $(8, 8)$, which equals four displacement wavelengths along each side of the plate; in other words, exactly two displacement wavelengths per FE. This mode frequency can be predicted within a tolerance of 2.5% (5% in eigenvalue) by using the FE model and a uniform p-extension equals 14. It is thus possible to resolve at least two displacement wavelengths in each element. An approximate upper frequency limit is given at 1615 Hz, for the 2×2 element FE model with p values in the interval $2 \leqslant p \leqslant 14$, with a chosen engineering tolerance of 10% in relative error in eigenfrequency. This eigenfrequency corresponds to the eigenmode wave numbers $(10, 10)$ and 2.5 wavelengths per element. This limit value is well below the value of 0.10, normally recommended in standard engineering FE applications. Note here also that (cf. Fig. 2) a tolerance of 8% in eigenfrequency ($\omega_m/2\pi$) corresponds to a tolerance of approximately 15% in eigenvalue λ_m.

It is well known that a high order of polynomial interpolations may cause a large condition number, which results in numerical problems and uncertainty in the solution. This may be one possible source of decreased rate of convergence for the 1% tolerance level, observed in Fig. 2. For this purpose we investigate the condition number of an unconstrained positive definite FE mass matrix. The result is translated and plotted in Fig. 3, in terms of expected number of

Table 1
Exact 3-D eigenfrequencies for the PMMA plate[a]

Mode number m	Wave numbers i, j	Eigenfrequency (Hz)
1	(1, 1)	16.7
4	(2, 2)	66.9
11	(3, 3)	150
20	(4, 4)	266
32	(5, 5)	415
48	(6, 6)	595
67	(7, 7)	806
90	(8, 8)	1047
115	(9, 9)	1317
143	(10,10)	1615

[a]With simply supported boundary conditions.

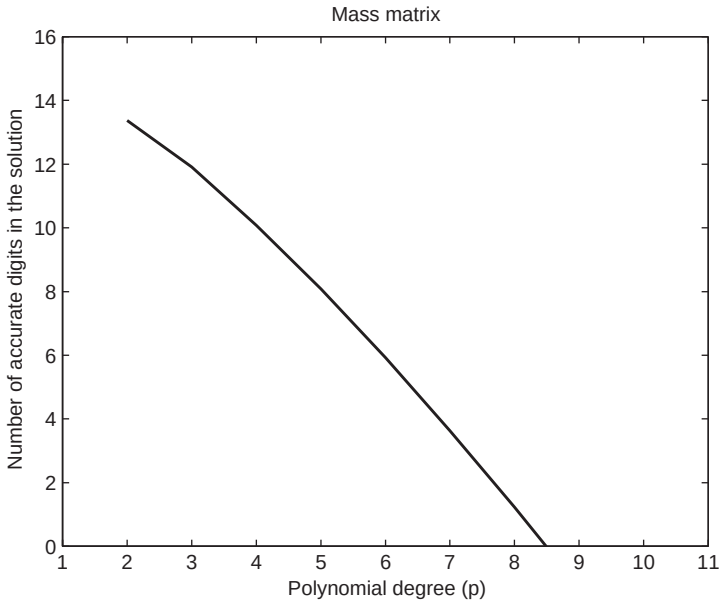

Fig. 3. The number of expected accurate digits in the solution with respect to the order of p in the polynomial approximation, related to the condition number of one unconstrained element mass matrix $\mathbf{M}$ as follows: $Nr = 16 - \log_{10}(\mathrm{cond}(\mathbf{M}(p)))$.

significant figures in the solution. It is clear that the use of $p > 8$ for an unsupported (free) structure is not meaningful. However, this boundary condition represents the worst case and consequently a better condition number is expected for other types of boundary conditions.

Finally, convergence plots are displayed for eigenmode number one in Fig. 4, and for eigenmode number 19 in Fig. 5. The solution is in this case regular and it is possible to reach the exponential convergence by using only p-enrichments. In the convergence plots, in Figs. 4 and 5,

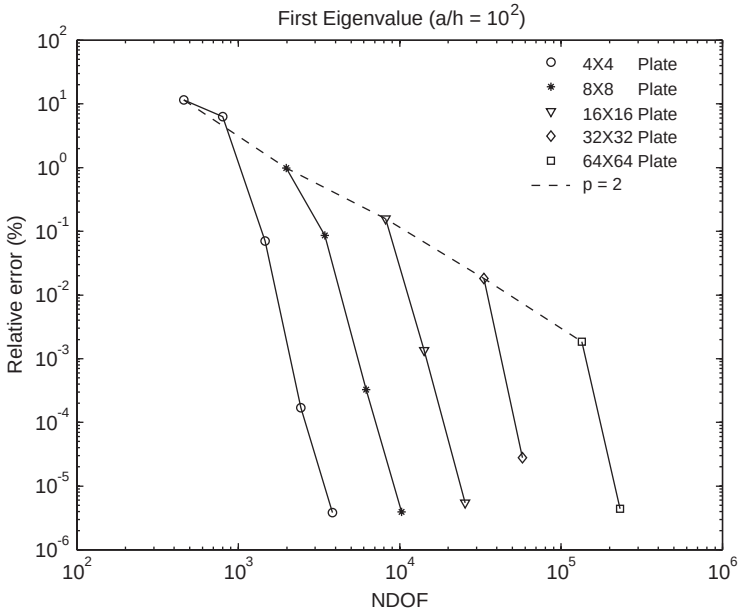

Fig. 4. Percentage relative error between first eigenvalue for the exact solution and the FE approximation versus number of degrees of freedoms spent using different *hp*-FE models for the normal case, $h = 10$ mm, with two elements through the thickness (4×4 circle, 8×8 star, 16×16 triangle, 32×32 diamond, 64×64 square and $p = 2$ dashed line).

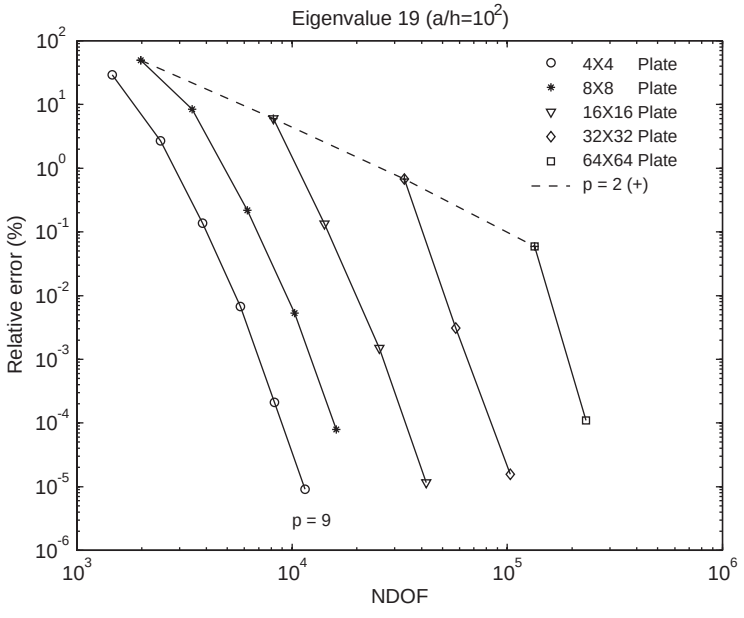

Fig. 5. Percentage relative error between eigenvalue number 19 for the exact solution and the FE approximation versus number of degrees of freedoms spent using different *hp*-FE models for the normal case, $h = 10$ mm, with two elements through the thickness (4×4 circle, 8×8 star, 16×16 triangle, 32×32 diamond, 64×64 square and $p = 2$ dashed line).

the h-refinement is uniform only in the plane of the plate. Two elements across the thickness are used throughout the study. The rate of convergence observed is thus slightly better than algebraic for uniform refinement in the plane of the plate. Fig. 5 shows that for any given accuracy, the p-enrichments are more efficient than h-refinements in terms of degrees of freedoms spent. This is coherent with theoretical and numerical observations in elastostatics for regular solutions [3]. A factor 40 is gained (Fig. 5) in terms of degrees of freedom spent compared to using uniform quadratic interpolation functions (p fixed at 2) already at a chosen accuracy of 10^{-1}.

3.2. Numerical locking problems in elasto-dynamics

It is well known that locking may cause serious problems in 3-D structural modelling using linear or quadratic FEs. The locking occurs when certain parameters tend to limit values, as for example, shear locking in thin domains or volumetric locking for nearly incompressible material. Locking problems are most often handled by using alternative variational formulations or reduced constraint methods [8,9]. It is also known that by using certain p-version elements it is possible to alleviate this problem [35]. Complete locking with the h-version FEM may occur in highly anisotropic domains, cf. [8]. One of the important issues in this section is to investigate (numerically) how locking effects can be alleviated in dynamics, by using higher-order polynomial interpolation functions [8–10]. It is recalled that the locking effect in general is a global property. Moreover, the conditioning number of the global system matrix may be even worse when using many elements, due to cancellation in the assembly process.

3.2.1. Shear locking in thin domains [36]

The numerical approximation of bending and shear dominated vibrations of thin plate- or shell-like domains may lead to shear locking when the thickness h is small. The standard procedure here is to change from a full 3-D continuum formulation to an approximate 2-D plate or shell formulation. In this paper, we numerically investigate the practical upper bound of the length to thickness aspect ratio for the 3-D continuum formulation, as it is important to account for 3-D effects near boundaries and joints. For this purpose only the elasto-dynamic problem is studied. In order to investigate the effects of shear locking, a set of thin plate-like structures is used with length to thickness aspect ratios given as $a/h = \{\,10^1 \quad 10^2 \quad 10^3 \quad 10^4\,\}$. The relative error in the first eigenvalue for the plate is calculated with different splits into four new elements using quadratic elements in each new level (so-called uniform h-refinement in the plane). The results from calculation of the relative error in the first eigenvalue for the $32 \times 32 \times 2$ elements FE model for different length to thickness aspect ratios (a/h) are plotted in Fig. 2. This FE model, with $32 \times 32 \times 2$ elements, is chosen in order to have a small discretisation error starting at p equals 2, while avoiding certain other numerical problems described in Section 3.1. With p equals 2, the error is fairly stable (Fig. 6) with respect to the a/h ratio up to 1000. However, and more importantly, from the dashed line in Fig. 8 it is obvious that uniform h-refinements with $p = 2$ will not converge at all. Improvement of the solution accuracy beyond 0.1% error may only be achieved by increasing the polynomial degree of the interpolation. The ultimate inhibition of h-convergence is here attributed to the so-called shear locking. The locking occurs when certain parameters tend to limit values, as for example shear locking in thin domains or volumetric locking for a nearly incompressible material. In terms of stresses or strains it may be even worse

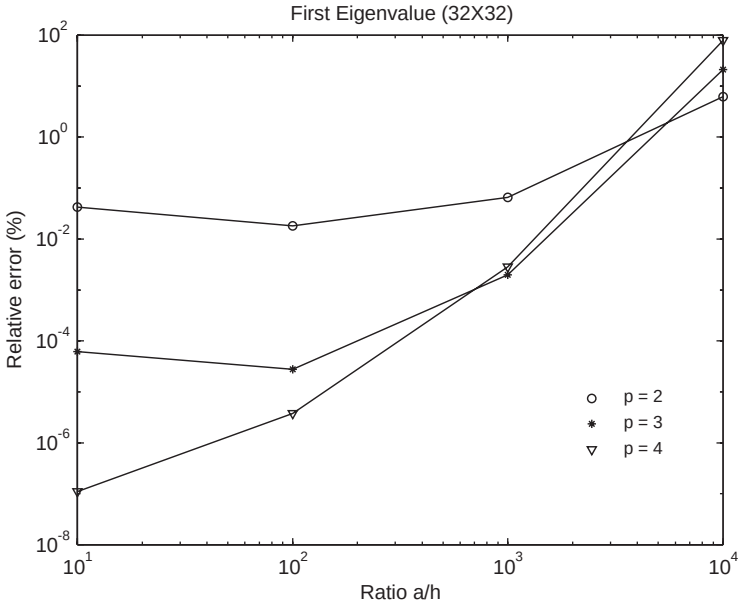

Fig. 6. Percentage relative error in eigenvalue between the exact solution and the FE approximation ($32 \times 32 \times 2$ elements, $p = 2$ circle, $p = 3$ star and $p = 4$ triangle) for different values of the length aspect ratio (a/h).

[8,9]. However, there is an upper limit for which the pure displacement-based p-version FEM is effective in handling the thin domain locking problem using 3-D continuum theory. According to Fig. 6, a/h should not exceed 1000 in practice.

3.2.2. *Volumetric locking or Poisson locking [36]*

One way to overcome volumetric locking problems in computations involving nearly incompressible materials is to use a mixed two field, pressure and displacement, variational formulation [9,10]. Such formulations provide means for constructing locking-free elements not only with respect to displacements but also with respect to stresses. In order to investigate the effects of volumetric locking, a set of plates with dimensions $1000 \times 1000 \times 10\,\text{mm}^3$ and different values on the Poisson's ratio $v = \{0.40\ \ 0.49\ \ 0.499\ \ 0.49999\ \ 0.499999\ \ 0.49999999\ \ 0.499999999\}$ are studied.

If we compare the result in accuracy of the first eigenvalue with respect to variations in Poisson's ratio, it is rapidly lost for each decimal 9 that is added. Each additional decimal figure on Poisson's ratio results in approximately one lost figure on the accuracy in the solution, according to Fig. 7. The first eigenvalue of a plate is clearly affected by locking when using Poisson's ratio $v = 0.49999999$. The result in Fig. 9 shows the accuracy in the first eigenvalue versus number of degrees of freedom for different values of p (see Figs. 8 and 9). The convergence properties for nearly incompressible materials show a global tendency that is very much like those found for thin domain locking, described in Section 3.2.1. The locking effect is a global property and the conditioning number of the system matrix may be even worse, by increasing the cancellation effect in the assembly process when using h-refinement. This effect is visible in Fig. 9

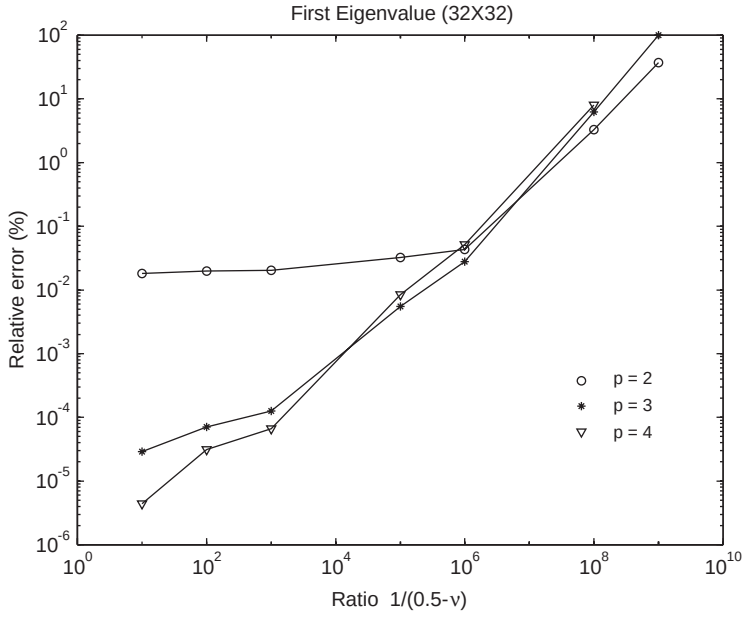

Fig. 7. Percentage relative error in eigenvalue between the exact solution and the FE approximation ($32 \times 32 \times 2$ elements, $p = 2$ circle, $p = 3$ star and $p = 4$ triangle) for different values of Poisson's ratio v.

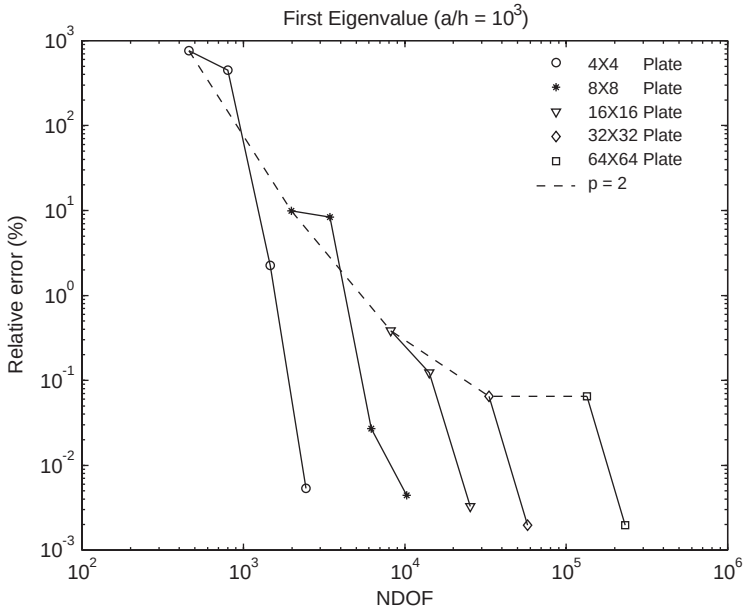

Fig. 8. Percentage relative error between the first eigenvalue for the exact solution and the FE approximation versus number of degrees of freedoms spent using different *hp*-FE models for $a/h = 10^3$ and two elements through the thickness (4×4 circle, 8×8 star, 16×16 triangle, 32×32 diamond, 64×64 square and $p = 2$ dashed line).

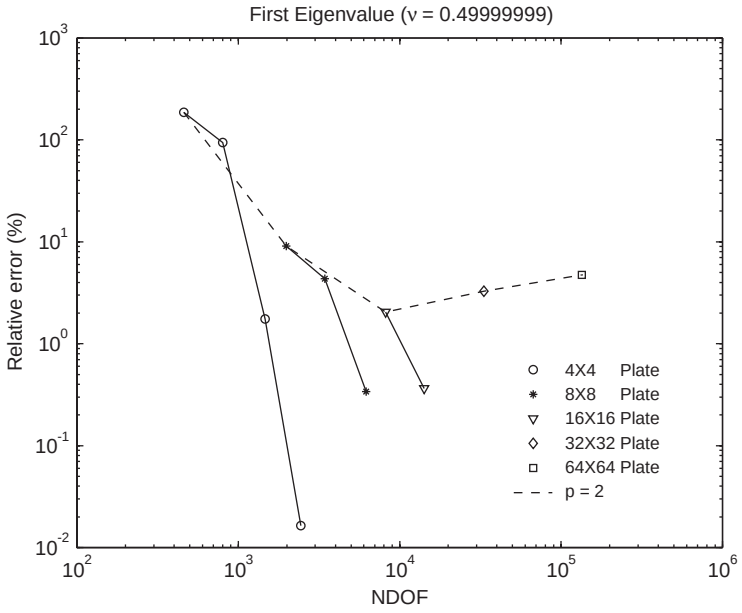

Fig. 9. Percentage relative error between eigenvalue for exact solution and the FE approximation versus number of degrees of freedoms spent using different *hp*-FE models for $v = 0.49999999$ and two elements through the thickness (4×4 circle, 8×8 star, 16×16 triangle, 32×32 diamond, 64×64 square and $p = 2$ dashed line).

with an increasing relative error with respect to two *h*-refinements (dashed line). The only possible way to alleviate the locking converge is to balance the number of elements and the order of interpolation. For the $32 \times 32 \times 2$ element FE model, with $v = 0.49999999$, there is no gain in solution accuracy from increasing the interpolation order p. Also in this case, there is a practical upper limit for which the pure displacement-based *p*-version FEM is effective in handling the volumetric locking problem by *p*-enrichments. Our results in Figs. 7 and 9 indicate that Poisson's ratios should not be closer to one half than 0.499999 when considering this approach.

3.3. Forced vibration frequency response of a viscoelastic simply supported plate

In a locking-free setting, the smoothness of the solution is the most important contributing factor to the rate of convergence. In the case of forced frequency response of real-life damped structures, the FE solution will in general be irregular due to sharp corners, edges and other geometric singularities. Boundary conditions, loadings and material discontinuities are other sources for solution irregularities. The case considered in this section includes a load singularity caused by a spatially constant distributed load applied over a rectangular area. In the present analysis, only non-optimal uniform *h*-refinements in the plane are used. Only uniform *p*-enrichments are used, which are also non-optimal in the presence of singularities. In order to handle the general case, including singularities, an *hp*-adaptive approach including a posteriori error estimation will be needed in order to obtain optimal (exponential) convergence rates.

Table 2
Estimated viscoelastic damping parameters for PMMA

Damping process number n	Relaxation frequency β_n (Hz)	Process amplitude $A_G^{(n)}$	Process amplitude $A_\lambda^{(n)}$
1	1.59×10^{-1}	2.23×10^{-1}	0.0
2	2.26×10^{-1}	2.21×10^{-1}	0.0
3	8.21×10^{1}	3.27×10^{-2}	0.0
4	3.14×10^{2}	1.00×10^{-4}	0.0
5	1.59×10^{-1}	1.32×10^{-1}	0.0

A simply supported $1000 \times 1000 \times 10\,\text{mm}^3$ PMMA plate, with material data given in Ref. [25] and Table 2, is used to show some aspects of discretisation error control. The excitation applied to the PMMA plate is given by a distributed $250 \times 250\,\text{mm}^2$ unit pressure load excitation at position $\mathbf{x}_e = \{375\ \ 375\ \ 0\}\,\text{mm}$, with respect to the lower left corner of the plate. A typical vibration frequency response function (FRF) for the PMMA plate in the frequency interval 1–1000 Hz, at point $\mathbf{x} = \{540\ \ 180\ \ 0\}\,\text{mm}$, is shown in Fig. 10, using a 4×4 element mesh with varying orders of polynomial degree of approximation (2, 3 and 6). With the 4×4 mesh, when p equals 2 it is only possible to simulate the frequency response up to approximately 50 Hz, which includes the first visible resonance. The use of polynomial degree $p = 6$ may be justified up to approximately 500 Hz. In order to cover the entire frequency interval 1–1000 Hz using the 4×4 mesh, it is necessary to use a p value equal to 9. In this case there is no longer any visual difference between the exact 3-D solution and the FE approximation. The mean relative difference in magnitude FRF is 0.12% and the standard deviation is 0.20%. Also, note that an accurate prediction of the vibration response solution at each anti-resonance frequency is very important as these frequencies correspond to high dynamic stiffness.

A convergence study is also performed on the PMMA plate at three different selected frequencies 19, 533 and 1047 Hz. The first frequency at 19 Hz corresponds to the first resonance frequency. The vibration displacement field is well approximated with all FE models in terms of the Nyquist sampling theorem. In Fig. 11, the relative error between exact 3-D solution and FE approximation is given for h-refinements and p-refinements, respectively. The dashed line corresponds to successive splits into four new elements in the plane using quadratic elements in each new level (so-called uniform h-refinement). The relative error between the exact solution and the FE approximation at the first frequency (19 Hz) declines rapidly at first and then levels out completely. This is due to the force singularity described above. For the second and third frequency, shown in Figs. 12 and 13, the situation is different. The rate of convergence is not retarded as for the first frequency. The solution error is composed of discretisation error and numerical error, due to the finite precision arithmetic. Using non-optimal h-refinements and p-enrichments, respectively, it is likely that we observe a growing numerical error with increasing p-order. It is also observed that the condition number of the dynamic stiffness matrix increases rapidly with increasing p-order and the numerical error may become visible for larger p-values. The results from the convergence studies at 533 and 1047 Hz, in Figs. 12 and 13, show that for vibration problems there is a very large potential in computational cost saving by using the p-version FEM. In Fig. 13, the decrease in error does not start until the Nyquist sampling

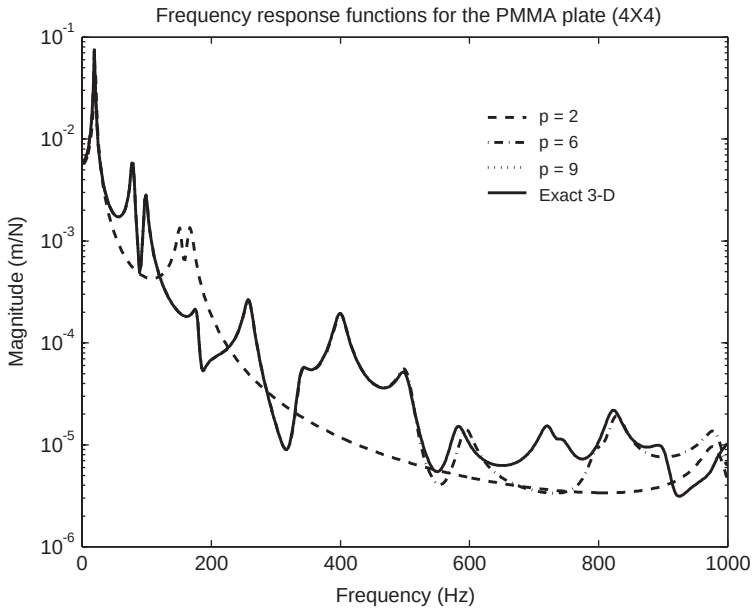

Fig. 10. Direct frequency response FE calculation for the PMMA plate using different orders of polynomial approximation (2 dashed, 6 dashed–dotted and 9 dotted line) and two elements through the thickness. The exact solution is also plotted for comparison (solid line).

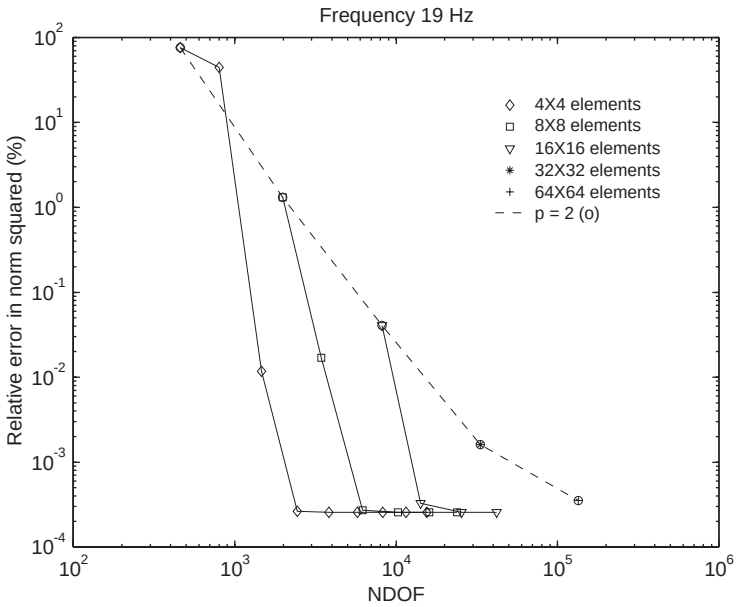

Fig. 11. Percentage relative error in energy norm between exact forced frequency response solution (at 19 Hz) and the corresponding FE approximation versus the number of spent degrees of freedoms, for different *hp*-FE models with two elements through the thickness (4×4 diamond, 8×8 square, 16×16 triangle, 32×32 star, 64×64 plus and $p = 2$ dashed line).

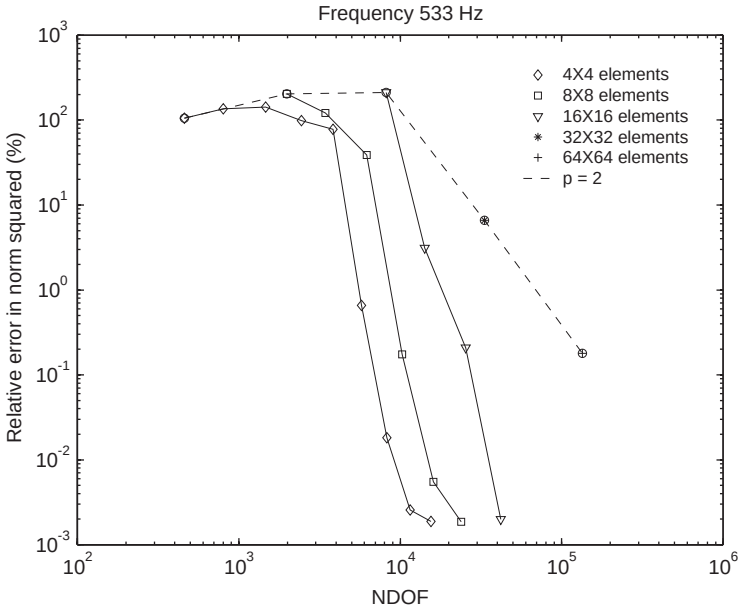

Fig. 12. Percentage relative error in energy norm between exact forced frequency response solution (at 533 Hz) and the corresponding FE approximation versus the number of spent degrees of freedoms, for different *hp*-FE models with two elements through the thickness (4×4 diamond, 8×8 square, 16×16 triangle, 32×32 star, 64×64 plus and $p = 2$ dashed line).

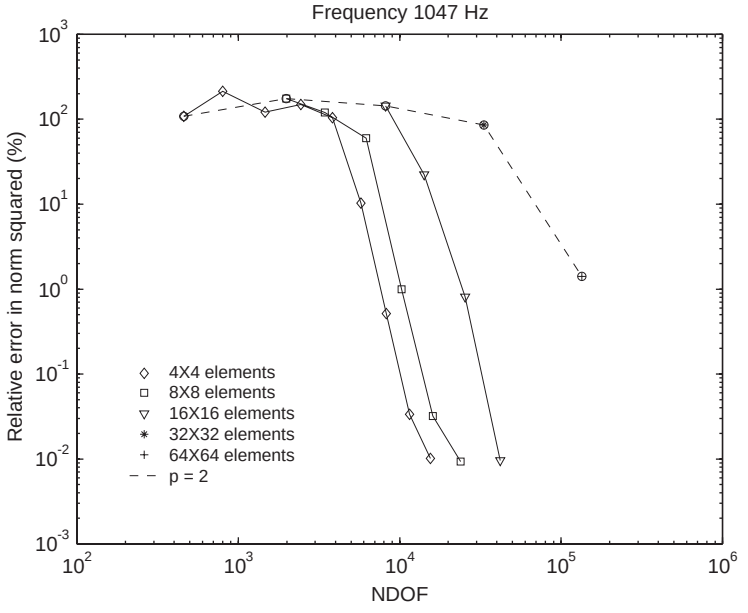

Fig. 13. Percentage relative error in energy norm between exact forced frequency response solution response (at 1047 Hz) and the corresponding FE approximation versus the number of spent degrees of freedoms, for different *hp*-FE models with two elements through the thickness (4×4 diamond, 8×8 square, 16×16 triangle, 32×32 star, 64×64 plus and $p = 2$ dashed line).

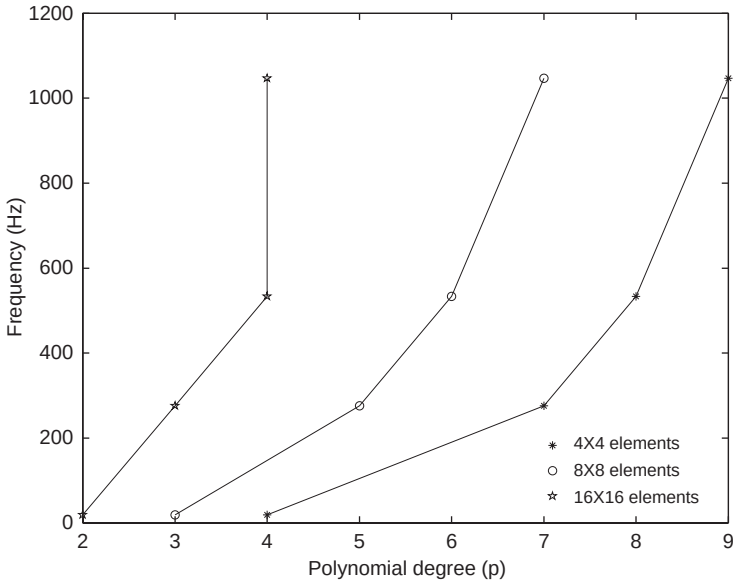

Fig. 14. Order of polynomial approximation p needed for a given relative error of 0.01% in forced frequency response energy norm (at frequencies 19, 276, 790 and 1047 Hz) for different h-refinements with two elements through the thickness (4×4 ****, 8×8 circle, 16×16 star).

theorem is fulfilled. Using h-refinements with p equals 2 this is achieved at about 35,000 degrees of freedom. If on the other hand p-enrichments are used instead, it is possible to have a relative error in norm below 0.1%, using 10,000 degrees of freedoms. If traditional h-version FEM is used, this level of accuracy would require the use of a vibration model with $O(10^6)$ degrees of freedom.

Finally, the result in Fig. 14 shows the potential of accurate approximation of the vibration frequency response at different frequencies using the p-version FEM, with a given level of accuracy. If we disregard numerical aspects, it is clear that it is highly efficient to increase the order of the polynomial interpolation function for accurate simulation of vibration frequency response in an increased frequency range.

4. An experimental case study

4.1. Two aluminium plates bonded by a viscoelastic damping layer

A laminate with previously estimated material data [28] is finally used to show some benefits of being able to vary the approximation order p. The experimental test plate consists of an aluminium base plate with dimensions $650 \times 500 \times 4\,\text{mm}^3$ and a smaller centred top plate with dimensions $450 \times 400 \times 2\,\text{mm}^3$. They are bonded together by a Scotchdamp^{TM} SJ-2015X viscoelastic polymer tape. The elastic material data are given as $E_{Al} = 72000\,\text{MPa}$, $E_{visco} = 0.01\,\text{MPa}$, $\nu_{Al} = 0.326$, $\nu_{visco} = 0.4999$, $\rho_{Al} = 2795\,\text{kg/m}^3$ and $\rho_{visco} = 975\,\text{kg/m}^3$. Isotropic material damping parameters for the Scotchdamp^{TM} SJ-2015X viscoelastic polymer are here

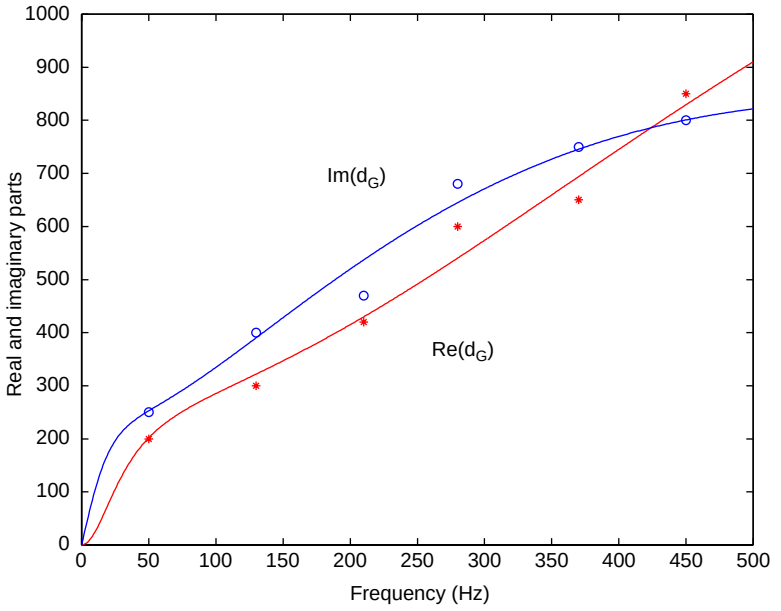

Fig. 15. Real and imaginary parts of parameterised viscoelastic isotropic material damping function (solid lines) and corresponding experimentally direct FE estimated values at each resonance, with real parts given by **** and imaginary parts by ○○○○.

given explicitly by nominal values at room temperature as $A_G^{(1)} = 269$, $A_G^{(2)} = 1650$, $\beta_1 = 200$ and $\beta_2 = 3936$. The corresponding isotropic complex material damping function is plotted in Fig. 15 [28].

The vibrations (normal velocities) were experimentally measured in the laboratory using a Laser–Doppler Vibrometer (LDV). A standard vibration transfer FRF measurement technique is used. Point receptances formally defined as quotients between the displacement field component spectra $\tilde{u}_i(\mathbf{x}, s)$ in direction i at response point $\mathbf{x}$ and corresponding point force component excitation spectra in direction k at point $\mathbf{x}_e$ on the boundary $\partial\Omega$ were recorded. The measurements were performed at room temperature, 24 °C. Each test plate was suspended during the measurements, with its face oriented vertically, by two long metal strings attached at the nodal lines of the first resonance to minimise suspension damping and simulate stress-free boundary conditions [37]. The non-contacting LDV sensor was chosen in order to minimise the influence of unwanted mechanical disturbances on the test objects. Excitation was imposed through a push-rod mounted electrodynamic shaker attached over a small surface centred at the excitation point. The vibration motion amplitude level, generated by the excitation, is kept much smaller than the thickness of the test specimen. The input force was applied normal to the surface of the test plate and measured by means of a standard force transducer, attached (glued) to the structure according to the setup in Fig. 3.15b in Ref. [37]. The effect of air damping and damping from the suspension may be neglected, cf. [38]. The laminate is excited by a distributed $15 \times 15\,\mathrm{mm}^2$ unit force spectrum excitation at position $\mathbf{x}_e = \{60\ \ 180\ \ 0\}\,\mathrm{mm}$, with respect to the lower left corner of the plate. The FE mesh is shown in Fig. 17 (see Figs. 16 and 17).

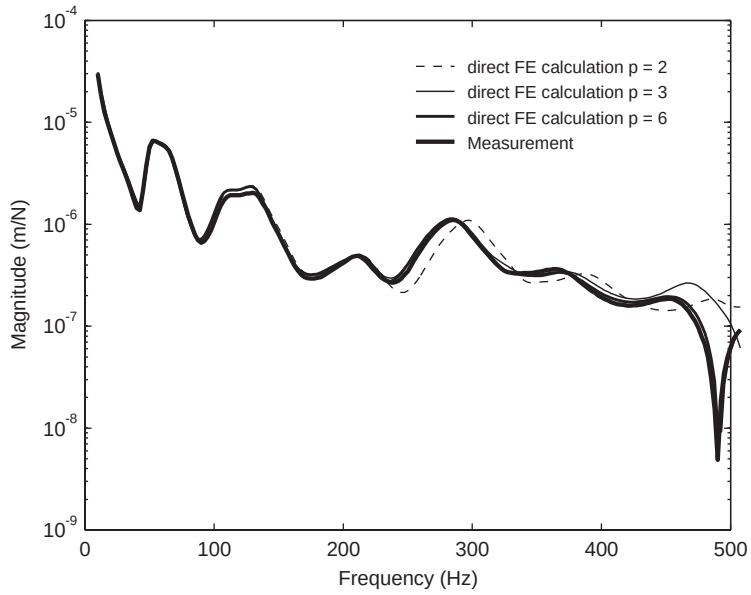

Fig. 16. Measured FRF for the aluminium laminate plate with embedded viscoelastic layer used for estimation and corresponding direct FE calculation using $p = 2$ dashed, 3 thin solid and 6 solid line.

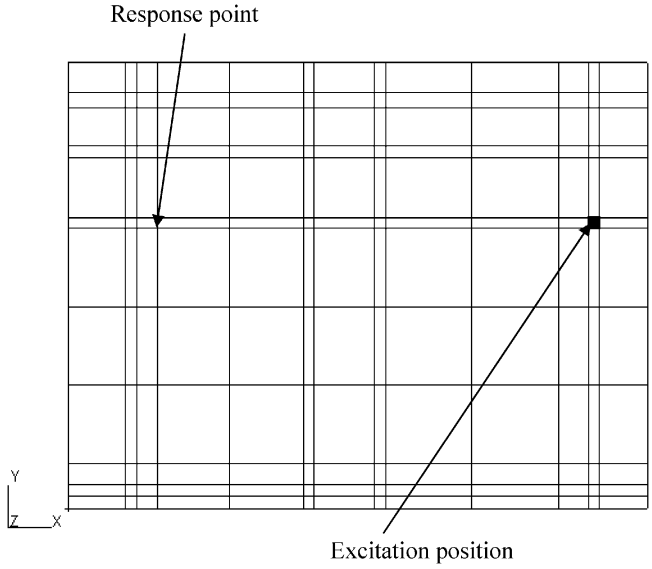

Fig. 17. The FE mesh for the laminate, a viscoelastic layer embedded by two aluminium plates, used in the experimental case study. Response and excitation positions are indicated by arrows.

A typical measurement FRF in the frequency interval of 10–500 Hz is shown in Fig. 16, for a randomly chosen point at $\mathbf{x} = \{750\ \ 250\ \ 10\}$ mm, and FE model simulations using different orders of polynomial degree of interpolation (2, 3 and 6). When using p equals 2 the visual agreement is

good up to 200 Hz. If the order of interpolation p is increased to 3 the frequency interval is extended to 300 Hz. In order to have a good visual agreement between model simulations and measured FRF in the whole frequency interval, a p value equals 6 is needed. It is then possible to accurately simulate the location of anti-resonance at 492 Hz also. The mean percentage absolute value of the relative difference between measured and simulated FRF in the frequency interval is 6%, with a maximum relative difference of 50% obtained at the anti-resonance at 492 Hz. However, it is important to keep in mind that the accuracy in amplitude is here also influenced by bias error due to the limited dynamic in the measurements.

5. Conclusions and future work

The capability of reliably solving 3-D time-harmonic vibration response problems in the low- and mid-frequency range using a pure displacement-based p-version FE-methodology is investigated. 3-D linear elastic and the viscoelastic continuum theories are used throughout. The ability to reliably model thin-layered structures and nearly incompressible materials is investigated in particular. Convergence studies are performed using a set of simply supported plate-like structures. An analytic continuum 3-D series solution due to Navier is used as reference. The reliability limits given by the pure displacement-based p-version FE-approach are determined numerically. The approach is shown to be effective for engineering purposes for length to thickness aspect ratios less than 1000 and for Poisson's ratios not closer to half than 0.499999. Polynomial enrichments are the key to the applicability of the pure displacement-based 3-D continuum approach. In addition to alleviating shear and volumetric locking problems, p-enrichments are, as expected, shown to be far more effective resolving time-harmonic responses as compared with standard h-type refinements. Our numerical results show that the Nyquist sampling theorem can be fulfilled by pure p-enrichments, that is, without a subsidiary condition on h-refinements. The polynomial approximation order, however, cannot be raised arbitrarily high. The condition number of the system matrix deteriorates with increasing order p. The mass contribution is shown responsible: p-orders above 10 are useless. A case study with measured FRFs is used to corroborate the approach put forward. The test laminate, consisting of two aluminium plates constrained by a thin viscoelastic polymer damping treatment, includes most of the difficulties addressed. The ability to suppress and control the discretisation error in viscoelastic material function estimation procedures is essential for building reliable material databases. The proposed approach can readily be used for such purposes provided that the limitations are obeyed. Future work will concern development of true hp-adaptive strategies and optimal continuum 3-D-based formulations for the constrained cases addressed herein, for example, the possibility of improving the matrix condition number by using anisotropic p-extensions. Also, issues of better-conditioned interpolation functions are a topic for future research.

Acknowledgement

The funding provided by the Swedish Defence Material Administration (FMV) is gratefully acknowledged.

Appendix A. The Navier exact 3-D solution for laminates

The exact frequency domain formulation of an orthotropic $a \times b$ laminate which has displacement field $\mathbf{u}$, symmetric stresses $\tilde{\sigma}_{ij} = \tilde{\sigma}_{ji}$ and strain $\tilde{\varepsilon}_{kl} = \tilde{\varepsilon}_{lk}$ tensor field in each point in the body $\mathbf{x} = [x_1 \ x_2 \ x_3]^{\mathrm{T}}$, given in Cartesian coordinate, is used to investigate the convergence properties of h- and p-version FEM. The frequency domain Navier's equation of motion, where $s = \mathrm{i}2\pi f$, $\mathrm{i}^2 = -1$ and f is the current frequency of vibration, is given by

$$-\operatorname{div}\tilde{\sigma} + s^2\rho\tilde{\mathbf{u}} = 0, \tag{A.1}$$

where solid viscoelastic constitutive behaviour is modelled in the frequency domain by using the elasto-viscoelastic correspondence principle $\tilde{\sigma} = [\mathbf{C}_\infty + \mathbf{C}_a(s)] : \tilde{\varepsilon}$, with the stress–strain relation given as $\tilde{\varepsilon}(\tilde{\mathbf{u}}) = \left[(\nabla \otimes \tilde{\mathbf{u}})^{\mathrm{T}} + \nabla \otimes \tilde{\mathbf{u}}\right]/2$.

Finally, simply supported boundary conditions are introduced at the four edges, that is, at $x_1 = 0$ and a: $\{u_2 \ u_3 \ \sigma_{11}\} = \mathbf{0}$, and at $x_2 = 0$ and b: $\{u_1 \ u_3 \ \sigma_{22}\} = \mathbf{0}$ for all x_3. Traction-free boundary condition on the bounding planes of the laminate in the case of eigenvalue analysis and $\sigma_{33} \neq 0$ in the case of vibration response due to an applied force in the vertical x_3 direction. Each ply has a thickness of h_k.

The ansatz for ply k in the laminate satisfying all conditions above is given as

$$\begin{aligned}\tilde{\mathbf{u}}^k(\mathbf{x},t) &= \sum_{m=1}^{\infty}\sum_{n=1}^{\infty}\mathbf{c}_{mn}^k(\mathbf{x})\cos(\omega t)\\ &= \sum_{m=1}^{\infty}\sum_{n=1}^{\infty}\begin{bmatrix} U_{mn}^k(x_3)\cos(\alpha_m x_1)\sin(\beta_m x_2)\\ V_{mn}^k(x_3)\sin(\alpha_m x_1)\cos(\beta_m x_2)\\ W_{mn}^k(x_3)\sin(\alpha_m x_1)\sin(\beta_m x_2)\end{bmatrix}\cos(\omega t),\end{aligned} \tag{A.2}$$

where $\tilde{\mathbf{u}}^k(\mathbf{x},t) = \left[\tilde{u}_1^k \ \tilde{u}_2^k \ \tilde{u}_3^k\right]^{\mathrm{T}}$, $\mathbf{c}_{mn}^k(\mathbf{x})$ are the generalised modal Fourier coefficients and $\alpha_m = m\pi/a$ and $\beta_m = n\pi/b$. By substitution of the ansatz into the equation of motion for the k laminate and introducing a set of state variables, a system of six coupled first-order ordinary differential equations is given as

$$\frac{\mathrm{d}\mathbf{Z}^k(x_3)}{\mathrm{d}z} = \mathbf{A}^k\mathbf{Z}^k(x_3),$$

where

$$\mathbf{Z}^k = \left[\begin{array}{cccccc} U_{mn}^k & \frac{\mathrm{d}U_{mn}^k}{\mathrm{d}z} & V_{mn}^k & \frac{\mathrm{d}V_{mn}^k}{\mathrm{d}z} & W_{mn}^k & \frac{\mathrm{d}W_{mn}^k}{\mathrm{d}z}\end{array}\right]^{\mathrm{T}}, \tag{A.3}$$

where the coefficient matrix $\mathbf{A}^k$ is defined in Ref. [33]. The general solution is given by

$$\mathbf{Z}^k = \mathbf{U}^k\mathbf{Q}^k\left(-h_k/2 \leqslant x_3 \leqslant h_k/2\right)\mathbf{B}^k, \tag{A.4}$$

where the matrix $\mathbf{U}^k$ and the diagonal matrix $\mathbf{Q}^k$ contain the eigenvectors and eigenvalues of the coefficient matrix $\mathbf{A}^k$, respectively, and $\mathbf{B}^k$ the unknown coefficients of the k ply. By forcing displacement continuity conditions and traction continuity conditions at each ply interface of the laminate as $\mathbf{D}^k\mathbf{Z}^k = \mathbf{D}^{k+1}\mathbf{Z}^{k+1}$, the frequency response, from a single

uniformly distributed pressure load P on a rectangular area $u \times v$, positioned at (η, ξ), is then given as [34]

$$\mathbf{K}\mathbf{B}^N = \begin{bmatrix} \mathbf{D}^1\mathbf{U}^1\mathbf{Q}^1(-h_1/2)\mathbf{S} \\ \mathbf{D}^N\mathbf{U}^N\mathbf{Q}^N(h_N/2) \end{bmatrix} \mathbf{B}^N = \mathbf{F}, \tag{A.5}$$

$$\mathbf{F} = \left[0 \quad \frac{16P}{\pi^2 mnuv} \sin\left(\frac{m\pi\,\xi}{a}\right) \sin\left(\frac{n\pi\,\eta}{b}\right) \sin\left(\frac{m\pi\,u}{2a}\right) \sin\left(\frac{m\pi\,v}{2a}\right) \quad 0 \quad 0 \quad 0 \quad 0 \right]^{\mathrm{T}}, \tag{A.6}$$

where $\mathbf{S}$ is a transfer matrix between top and bottom ply, $\mathbf{B}^1 = \mathbf{S}\mathbf{B}^N$. For determination of the laminate's natural frequencies, the singular values of the system matrix $\mathbf{K}$ are determined.

References

[1] O.C. Zienkiewicz, Achievements and some unsolved problems of the finite element method, *International Journal for Numerical Methods in Engineering* 47 (2000) 9–28.

[2] R.S. Langley, N.S. Bardell, A review of current analysis capabilities applicable to the high frequency vibration prediction of aerospace structures, *The Aeronautical Journal* 2371 (1998) 287–297.

[3] B. Szabó, I. Babuška, *Finite Element Analysis*, Wiley, New York, 1991.

[4] P. Solin, K. Segeth, I. Dolezel, *Higher-Order Finite Element Methods*, Chapman & Hall/CRC Press, London, 2003.

[5] M. Ainsworth, J.T. Oden, *A Posteriori Error Estimation in Finite Element Analysis, Pure and Applied Mathematics*, Wiley, New York, 2000.

[6] P. Ladevèze, J.P. Pelle, Estimation of discretization errors in dynamics, *Computers and Structures* 81 (2003) 1133–1148.

[7] J.T. Oden, L. Demkowicz, W. Rachowicz, T.A. Westermann, Towards a universal *h–p* adaptive finite element strategy, Part 2. A posteriori error estimation, *Computer Methods in Applied Engineering* 77 (1989) 113–180.

[8] M. Suri, Analytical and computational assessment of locking in the *hp* finite element method, *Computer Methods in Applied Mechanics and Engineering* 133 (1996) 347–371.

[9] L. Chilton, M. Suri, Locking-free mixed *hp* finite element for curvilinear domains, *Computer Methods in Applied Mechanics and Engineering* 190 (2001) 3427–3442.

[10] T.-Y. Rong, A.-Q. Lu, Generalized mixed variational principles and solutions of ill-conditioned problems in computational mechanics: Part I. Volumetric locking, *Computer Methods in Applied Mechanics and Engineering* 191 (2001) 407–422.

[11] J.M. Melenk, On condition numbers in *hp*-FEM with Gauss–Lobatto-based shape functions, *Journal of Computational and Applied Mathematics* 139 (2002) 21–48.

[12] J.M. Melenk, K. Gerdes, C. Schwab, Fully discrete *hp*-finite elements: fast quadrature, *Computer Methods in Applied Mechanics and Engineering* 190 (1996) 4339–4364.

[13] N.S. Bardell, J.M. Dunsdon, R.S. Langley, Free vibration of coplanar sandwich panels, *Composite Structures* 38 (1997) 463–475.

[14] J. Nicolas, O. Beslin, A hierarchical functions set for predicting very high order plate bending modes with any boundary conditions, *Journal of Sound and Vibration* 202 (5) (1997) 633–655.

[15] A. Houmat, An alternative hierarchical finite element formulation applied to plate vibrations, *Journal of Sound and Vibration* 206 (2) (1997) 201–215.

[16] M. Barrette, A. Berry, O. Beslin, Vibration of stiffened plates using hierarchical trigonometric functions, *Journal of Sound and Vibration* 235 (5) (2000) 727–747.

[17] A. Houmat, A sector fourier p-element applied to free vibration analysis of sectorial plates, *Journal of Sound and Vibration* 243 (2) (2001) 269–282.

[18] G.W. Wei, Y.B. Zhao, Y. Xiang, A novel approach for the analysis of high-frequency vibrations, *Journal of Sound and Vibration* 257 (2) (2002) 207–246.

[19] J.C. Simo, T.J.R. Hughes, *Computational Inelasticity, Interdisciplinary Applied Mathematics*, Springer, New York, 1998.
[20] C.T. Sun, Y.P. Lu, *Vibration Damping of Structural Elements*, Prentice Hall PTR, Englewood Cliffs, NJ, 1995.
[21] S.J. Hwang, R.F. Gibson, The effect of three-dimensional states of stress on damping of laminated composites, *Composite Science and Technology* 41 (1991) 379–393.
[22] K. Dovstam, Simulation of damped vibrations based on augmented Hooke's law and elastic modes of vibration, *International Journal of Solids Structures* 37 (2000) 5413–5445.
[23] K. Dovstam, Augmented Hooke's law based on alternative stress relaxation models, *Research Journal of Computational Mechanics* 26 (2000) 90–103.
[24] M. Dalenbring, Damping function estimation based on measured vibration frequency responses and finite-element displacement modes, *Mechanical Systems and Signal Processing* 13 (4) (1999) 547–569.
[25] M. Dalenbring, Validation of estimated isotropic viscoelastic material properties and vibration response prediction, *Journal of Sound and Vibration* 265 (2003) 269–287.
[26] M. Dalenbring, Experimental material damping estimation for planar isotropic laminate structures, *International Journal of Solids Structures* 39 (2002) 5053–5079.
[27] M. Dalenbring, Experimental estimation of homogeneous material damping for composite laminate structures with planar isotropic isotropy, *Euromech 437 Colloquium*, Prague, Czech Republic, FOI-S-0523-SE, 2002.
[28] M. Dalenbring, A. Zdunek, Experimental material damping for laminate structures, *Tenth International Congress on Sound and Vibration*, 7–10 July, Stockholm, Sweden, 2003.
[29] B. Andersson, U. Falk, R. Jarlås, Self-adaptive FE-analysis of solid structures, Part I: element formulation and a posteriori error estimation, FFA TN 1986-27, The Aeronautical Research Institute of Sweden (FFA), Stockholm, 64pp, 1986.
[30] A.G. Peano, et al., Adaptive approximations in finite element structural analysis, *Computers & Structures* 10 (1979) 333–342.
[31] B.A. Szabo, A.G. Peano, Hierarchic finite elements, Report WU/CCM-83/1, Washington University, St. Louis, 1983.
[32] B.A. Szabo, G.J. Sahrmann, Hierarchic plate and shell models based on *p*-extension, *International Journal for Numerical Methods in Engineering* 26 (1988) 1855–1881.
[33] A. Nosier, R.K. Kapania, J.N. Reddy, Free vibration analysis of plates using a layerwise theory, *AIAA Journal* 31 (12) (1993) 2335–2346.
[34] S.P. Timoshenko, S. Woinowsky-Krieger, *Theory of Plates and Shells*, McGraw-Hill International, Singapore, 1959.
[35] A. Côté, C. François, On the selection of *p*-version shape functions for plate vibration problems, *Computers and Structures* 79 (2001) 119–130.
[36] K.-J. Bathe, *Finite Element Procedures*, Prentice-Hall, Englewood Cliffs, NJ, 1996.
[37] N.M.M. Maia, J.M.M. Silva, J. He, N.A.J. Lieven, R.M. Lin, G.W. Skingle, W.-M. To, A.P.V. Urgueria, *Theoretical and Experimental Modal Analysis*, Research Studies Press, Ltd., Baldock, Hertfordshire, England, 1997.
[38] B.E. Read, G.D. Dean, *The Determination of Dynamic Properties of Polymers and Composites*, Wiley, New York, 1978.